Characterizing electrostatic turbulence in tokamak plasmas with high MHD activity

2010 J. Phys.: Conf. Ser. 246 012014

(http://iopscience.iop.org/1742-6596/246/1/012014)

Journal of Physics: Conference Series **246** (2010) 012014 doi:10.1088/1742-6596/246/1/012014

Characterizing electrostatic turbulence in tokamak plasmas with high MHD activity

Z. O. Guimarães-Filho[1,2], G. Z. dos Santos Lima[1], I. L. Caldas[1], R. L. Viana[3], I. C. Nascimento[1], and Yu. K. Kuznetsov[1]

[1] Instituto de Física, Universidade de São Paulo, Caixa Postal 66316, 05315-970, São Paulo, SP, Brazil

[2] Equipe DSC/PIIM, Université de Provence UMR6633, F-13397 Marseille cedex 20, France

[3] Departamento de Física, Universidade Federal do Paraná, Caixa Postal 19044, 81531-990, Curitiba, PR, Brazil.

E-mail: viana@fisica.ufpr.br

Abstract. One of the challenges in obtaining long lasting magnetic confinement of fusion plasmas in tokamaks is to control electrostatic turbulence near the vessel wall. A necessary step towards achieving this goal is to characterize the turbulence level and so as to quantify its effect on the transport of energy and particles of the plasma. In this paper we present experimental results on the characterization of electrostatic turbulence in Tokamak Chauffage Alfvén Brésilien (TCABR), operating in the Institute of Physics of University of São Paulo, Brazil. In particular, we investigate the effect of certain magnetic field fluctuations, due to magnetohydrodynamical (MHD) instabilities activity, on the spectral properties of electrostatic turbulence at plasma edge. In some TCABR discharges we observe that this MHD activity may increase spontaneously, following changes in the edge safety factor, or after changes in the radial electric field achieved by electrode biasing. During the high MHD activity, the magnetic oscillations and the plasma edge electrostatic turbulence present several common linear spectral features with a noticeable dominant peak in the same frequency. In this article, dynamical analyses were applied to find other alterations on turbulence characteristics due to the MHD activity and turbulence enhancement. A recurrence quantification analysis shows that the turbulence determinism radial profile is substantially changed, becoming more radially uniform, during the high MHD activity. Moreover, the bicoherence spectra of these two kinds of fluctuations are similar and present high bicoherence levels associated with the MHD frequency. In contrast with the bicoherence spectral changes, that are radially localized at the plasma edge, the turbulence recurrence is broadly altered at the plasma edge and the scrape-off layer.

1. Introduction

Electrostatic turbulence is the main cause of the anomalous particle and energy transport at the plasma edge in tokamaks [1]. Usually the standard linear spectral analysis provides information about the waves at the plasma edge and the particle transport driven by these waves [2, 3]. In many tokamak experiments the correlation between the magnetic oscillations and the electrostatic turbulence is not significant [4]. However, this correlation turns to be relevant in new high-confinement regimes achieved in tokamaks [5, 6, 7, 8]. A number of experiments in tokamaks indicate that, under certain conditions, electrostatic turbulence can be modulated by Mirnov oscillations [9, 10, 11, 12, 13]. During L-H transitions in the Joint Experiment Tokamak

(JET) abrupt changes in the electric and magnetic fluctuation spectra have been observed [14]. Sudden changes in the spectra also appeared on the drift flow driven turbulence in the Large Plasma Device (LAPD) [15].

In the Tokamak Chauffage Alfvén Brésilien (TCABR) the magnetic and electrostatic frequency spectra present a peculiar partial superposition, in contrast with most tokamaks, for which such spectra are rather separated [13]. This fact might enhance the coupling, normally small, between these two kinds of fluctuations and opens the possibility of investigating this coupling. Moreover, in some TCABR regimes, the MHD activity increases at different instants of time during the discharge, and reaches high amplitudes with a narrow wave-number spectrum and a well-defined peak on the Mirnov frequency of $\sim$ 13 kHz [13, 16, 17, 18]. This increase of MHD activity occurs for two different kinds of discharge regimes [17]. In the first one, the MHD activity enhancement is observed only after the activation of a biased electrode, while in the second regime, the MHD activity increases spontaneously following changes in the edge safety factor [17]. For both regimes, the electrostatic turbulence is also much affected during the high MHD activity [16, 17, 18]. In previous works, some dynamical tools were applied to study the turbulence alterations. Namely, for the first regime a synchronization of the turbulence on the MHD frequency was observed [18], while the bicoherence enhancement was reported for the second regime [19].

Since magnetic oscillations (MHD activity) cause variations of plasma parameters, including density, temperature, and potential, an influence of these oscillations on the electrostatic fluctuations is naturally expected, depending on the strength of the MHD behavior. Usually, the fluctuating magnetic and electric fields show quite different frequency spectra without synchronization evidences between these two kinds of oscillations, as clearly shown, for example, in Figure 5 of Reference [20]. However, it is possible to distinguish the floating potential fluctuations with a broadband frequencies from those with the MHD frequencies [20, 21, 22]. In this sense, the synchronization in TCABR studied in this article could be considered as a peculiar relation between the high MHD activity and the electrostatic turbulence when the spectra of fluctuating magnetic and electric fields are partially superimposed.

The purpose of this article is to systematically describe dynamical alterations on the electrostatic turbulence observed with high MHD activity in the mentioned second TCABR regime. To do that, we apply some mathematical procedures used to identify dynamical characteristics on the turbulence time series. We use the recurrence quantification analysis and the bicoherence spectral analysis to evaluate the alterations in the radial profiles of the analyzed turbulence data. The turbulence data considered here are the floating potential fluctuations measured by Langmuir probes that will be also referred to as electrostatic turbulence. Initially we present experimental evidence of electrostatic turbulence synchronization at the Mirnov frequency, during high MHD activity in the second regime of the TCABR discharges (characterized by a spontaneous increase of MHD activity).

After that, we introduce an approach based on recurrences to study the turbulence dynamical alterations with high MHD activity, the recurrence quantification analysis (RQA) [23, 24, 25, 26]. This method is based on the so-called *recurrence plot* (RP), which is a plot showing, for a given time, the times at which a state changing its position in phase space, visits roughly the same area in the phase space. Recurrence plots have been introduced as a tool to calculate the maximum Lyapunov exponent related to a time series [27]. Later it has been shown that RPs can also be used to study non-stationarity of a time series as well as to indicate its degree of aperiodicity [28]. The quantitative characterization of recurrence plots, or recurrence quantification analysis (RQA), became an extremely useful tool in nonlinear time series analysis [29], and has been used in many applications ranging from meteorology [30], finance [31], and geophysics [32] to cardiology [33]. In particular, RPs have become important to characterize data from space [34] and fusion plasmas [24, 25, 26].

Turbulence can have recurrent behavior, as periodicities, and irregular variations. The RQA quantifies the recurrent structures in a given time series, indicating states which are again arbitrarily close after some time. This is a fundamental property of nonlinear systems [23]. We use RQA to evaluate the radial dependence of the recurrence alterations on the turbulence. For the turbulence with high MHD activity, we found changes in the recurrence structures of floating potential fluctuations in all the analyzed region. Thus, significant recurrence structures are found both in the plasma edge and in the scrape-off layer during the high MHD activity.

Furthermore, in order to complement the description of the turbulence dynamical alterations during the high MHD activity we apply the bicoherence spectral analysis to quantify the intensity of the electrostatic turbulence synchronization as well as its radial dependence. We observe that the turbulence bispectrum is much modified during the high MHD activity and, consequently, presents the same regularity of the magnetic oscillations with high bicoherence between the dominant Mirnov frequency and the remaining broadband spectrum frequencies. This high bicoherence is most pronounced near the plasma edge position around the rational magnetic surface with the safety factor $q = 3$. The result about bispectral analysis of the turbulence alterations during high MHD activity was partially published in [19], but it was included here in order to point out the differences in the turbulence radial profile alterations that can be detected when using the recurrence-based and the bispectral methods.

The rest of the paper is organized as follows: in the second Section we describe the TCABR experimental setting and the main alterations on turbulence fluctuations during high MHD activity. Section III treats the recurrence plots and the corresponding recurrence quantification analysis, as well as its application to the turbulence measured in the TCABR during ambient and high MHD activity. In Section IV we present the turbulence bicoherence analysis. The last Section contains our conclusions.

2. Experimental setup

The experiments have been done in the hydrogen circular plasma of the Brazilian tokamak TCABR [16] (major radius $R = 61$ cm and minor radius $a = 18$ cm). The plasma current reaches a maximum value of 100 kA, with duration 100 ms, the hydrogen filling pressure is 3×10^{-4} Pa, and toroidal magnetic field $B_0 = 1.1$ T. At the plasma edge the electron plasma density is $n_e \approx 3 \times 10^{18}$ m^{-3}, and the electron temperature is $T_e \approx 10$ eV. The floating electrostatic potential has been measured in the region comprising the plasma edge and the scrape-off layer ($0.9 < r/a < 1.2$) by a set of three movable electrostatic probes. Two of them were placed in two poloidal positions separated by 0.4 cm, yielding the floating potentials, φ_1 and φ_2, at the corresponding positions. The third probe, used to measure the ion saturation current I_S, was placed at a toroidal position 0.4 cm apart from the poloidal probes. The whole set was mounted at the equatorial region of the tokamak. Magnetic fluctuations were detected using a Mirnov coil located at $r = 19.5$ cm (i.e., 1.5 cm outside the plasma radius). Radial profiles of electrostatic fluctuations were obtained on shot-to-shot basis. Probe and Mirnov coil data were digitized at 1.00 and 0.25 megasample per second, respectively, and filtered to avoid anti-aliasing filter.

Figure 1 shows the time evolution of a typical example of the plasma discharge in TCABR that have been considered in this work. The plasma current [Fig. 1(a)] grows rapidly in the first milliseconds until ~ 50 kA, then increases at a slower rate until reaching a short plateau where the current stays at a 100 kA level, decaying slowly during the second half of the discharge. The central chord-integrated electron density, indicated by Fig. 1(b), exhibits a similar evolution, with a first plateau level of $n_e \sim 1.0 \times 10^{19}$ m^{-3} which roughly coincides with the slower current ramp, and is followed by a second plateau of $\sim 1.2 \times 10^{19}$ m^{-3} between 42 ms and 60 ms. During the rest of the discharge the density decreases gently until disruption. It is interesting to observe that during this second (and higher) plateau of the plasma density the magnetic activity is high.

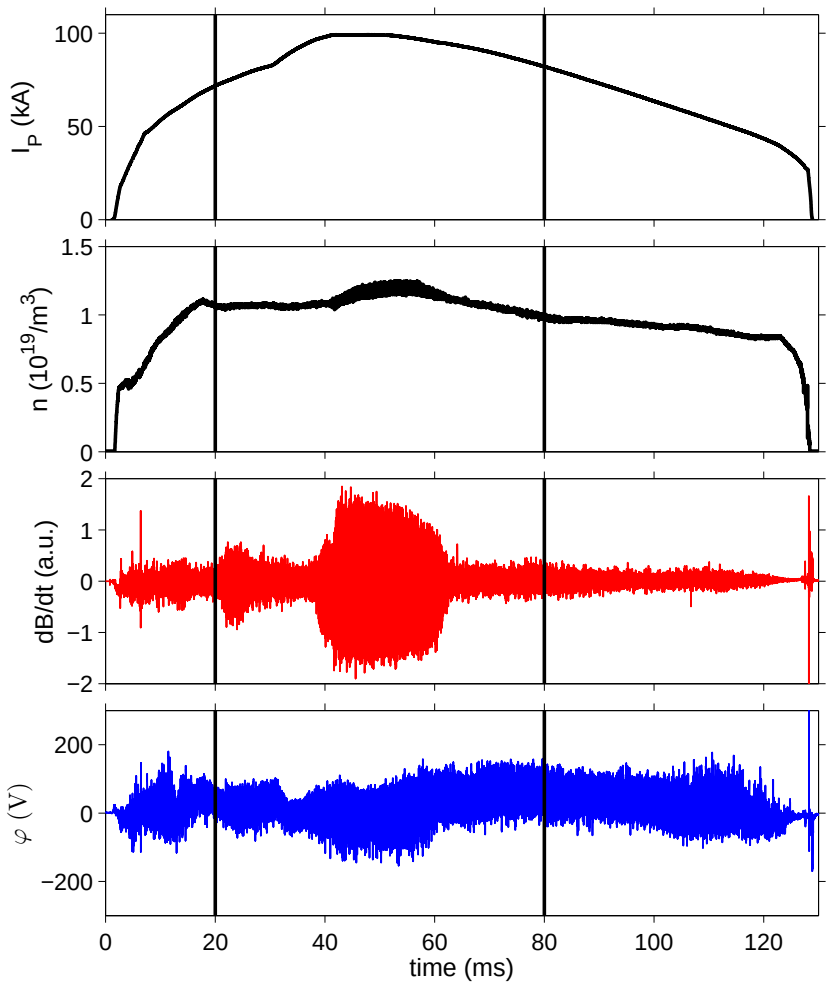

Figure 1. (color online) Time evolution of the (a) plasma current, (b) central chord-integrated plasma density, (c) MHD activity, and (d) floating potential (at $r_S/a = 0.92$) for a discharge (# 18369) of TCABR tokamak with bias polarization.

The MHD activity measured by the coils, or the fluctuations of the poloidal field time rate, $\dot{\tilde{B}}$, are depicted in Fig. 1(c). It is interesting to observe that, during this discharge, the MHD activity grows in two stages. A little increase around 22 ms occurs when the edge safety factor at plasma edge reaches the integer value $q(a) = 4$ (and have dominant poloidal mode $m = 4$). The more strong growth of MHD activity observed around 40 ms has, in fact, two saturated stages: the first one starts to grow at *circa* 38 ms when $q(a) \approx 3$ (and the dominant poloidal mode is $m = 3$ [17] and evolves to a more intense second stage at $\sim$ 42 ms. This second stage, more strong and reproducible, will be analyzed in this work. After these events the magnetic activity is reduced to a noisy level. Fig. 1(d) shows the time evolution of the floating electrostatic potential φ_1 along the discharge. During the burst of magnetic activity started at 42 ms, important dynamical characteristics of the electrostatic fluctuation are strongly affected, as it will be shown later along this article. Moreover we find that, after the magnetic burst ceases, the electrostatic fluctuations resume to their former behavior with respect to these characteristics, but with different mean and standard deviation values.

The Fourier spectra of both magnetic and electrostatic fluctuations are depicted in Fig. 2

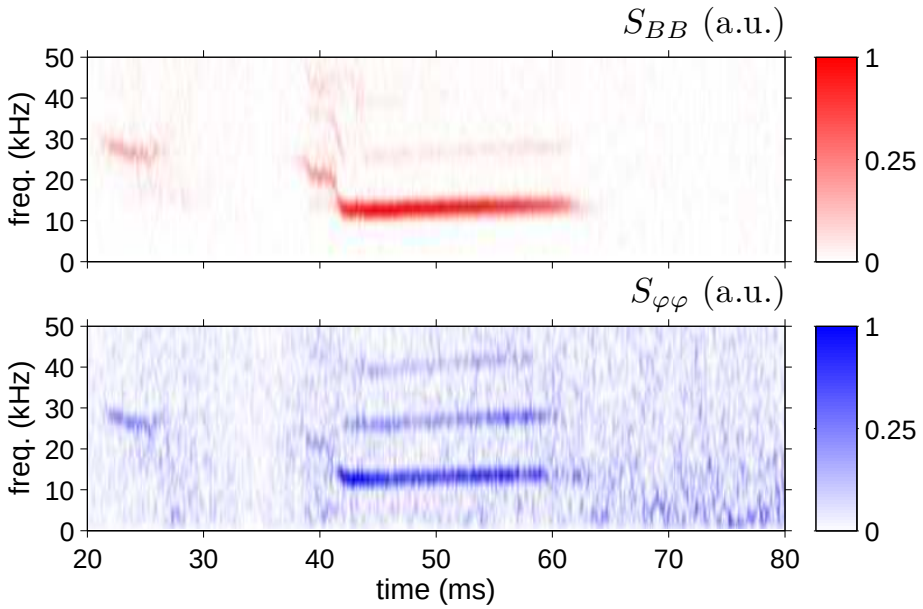

Figure 2. (color online) Fourier power spectral density (arbitrary units) for Mirnov oscillations (a) and electrostatic potential (b) at $r_S/a = 0.94$ during the discharge of Fig. 1.

for magnetic data and electrostatic measurements performed at a fixed radius $r = 17$ cm. In the spectrograms, the oscillation frequencies are plotted against the discharge duration, the corresponding power spectral densities (in arbitrary units) being plotted in a color scale. Figure 2(a) exhibits the spectrogram for Mirnov oscillations, where the periods of magnetic activity are associated with peaks of the power spectral density S_{BB}. In particular, the intense burst started at 42 ms has a sharp line with a dominant frequency of ~ 13 kHz which extends up to 60 ms, with at least two overtones corresponding to higher harmonics of the dominant frequency. The modulation in the electrostatic potential fluctuation can be seen in [Fig. 2(b)], where its spectrum presents peaks (or lines for running time) at the same frequencies of the magnetic fluctuations. It is interesting to note that the MHD activity at 22 ms, related to $q(a) \approx 4$, also modulates the floating potential fluctuations.

In addition, we verified a phase-locking between signals measured at different poloidal positions by computing the phase angle θ_{12} related to the cross-spectrum of the potential fluctuations, $\tilde{\varphi}_1(t)$ and $\tilde{\varphi}_2(t)$, measured at different poloidal positions of the plasma column (separated by 0.4 cm). The spectrogram of this phase angle is exhibited in Fig. 3(a), showing an interval for which the angle is nearly constant for the same base frequency of MHD activity f_{MHD}. Moreover, the spectrogram of phase angle between one of these signals and Mirnov oscillations [Fig. 3(b)] is another indication that this synchronization is driven by the MHD activity. Is important to mention, that similar behavior was also observed for the ion saturation current fluctuations (which are proportional to the local plasma density fluctuations, provided the temperature fluctuations are not taken into account).

The electrostatic turbulence synchronization at the MHD frequency can be characterized in a more quantitative way by considering the so-called order parameter, which is a well-known diagnostic of synchronization in problems of nonlinear dynamics [35, 36]. Let θ_{12} be the phase angle obtained from the cross-spectrum of the signals of the two Langmuir probes measuring

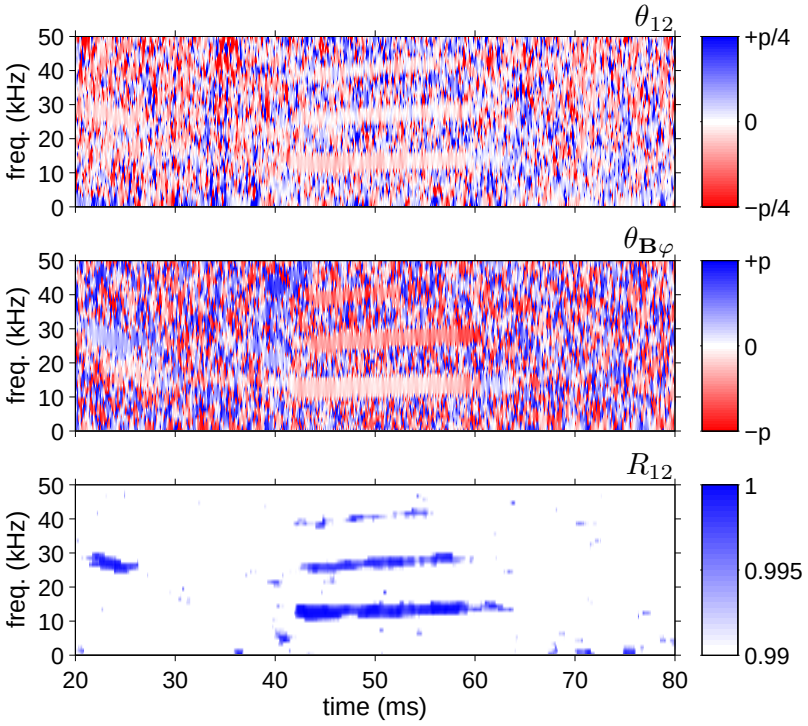

Figure 3. (color online) Spectrogram showing the time evolution of the spectral properties of (a) phase angle between floating potential data sampled at different poloidal locations and $r/a = 0.92$. (b) phase angle between magnetic oscillations and floating potential fluctuations measured at $r/a = 0.92$. (c) Time evolution of the order parameter magnitude computed for the phase angles between floating potential data sampled at different poloidal locations and $r/a = 0.92$.

floating potential, $Vf_1(t)$ and $Vf_2(t)$. The corresponding order parameter is defined as

$$R_{12}(t,f) = \left| \left\langle e^{i\theta_{12}} \right\rangle_t \right|, \tag{1}$$

which is the magnitude of a centroid phase vector, and the time average

$$\left\langle e^{i\theta_{12}} \right\rangle_t = \frac{1}{\Delta t} \int_{-\Delta t/2}^{\Delta t/2} e^{i\theta_{12}(\tau+t,f)} d\tau, \tag{2}$$

is computed over an interval of duration $\Delta t = 1.5$ ms, which is a convenient interval to obtain the order parameter with a good precision (that requires Δt to be some integer multiples of the window size used to compute the Fourier spectrogram), but the interval is small enough to allow analyzing the parameter evolution.

A completely synchronized state is such that the centroid vector is the coherent sum of all phase vectors, thus giving $R_{12} = 1$. Non-synchronized states, in general, are characterized by lower values of the order parameter. A spectrogram of the Mirnov oscillations [Fig. 2(a)] can be compared with that obtained for the order parameter magnitude $R_{12}(f)$ [Fig. 3(c)] of the floating potentials measured at two different poloidal positions. The order parameter allows us to identify the intervals and frequencies for which this synchronization occurs. A clearly noticeable

synchronization band appears in the phase spectrogram, reinforcing our previous claims. Note in Fig. 3 that the early growth of MHD activity at 22 ms also leads to a temporary phase synchronization similar to the one discussed before.

3. Characterization of turbulence using dynamical recurrences

3.1. Recurrence plots

Let us suppose that an experiment yields an univariate time series obtained from measurements of a single physical variable $x_i = x(t = i\Delta)$ at a given point of space, where Δ is the inverse sampling frequency, and $i = 1, 2, \ldots N$ (N is the total number of points). An example is the floating potential measured by a probe inserted somewhere within the plasma tokamak edge. We make an embedding using the vectors [37].

$$\mathbf{x}_i = \{x_i, x_{i+\tau}, x_{i+2\tau}, \cdots, x_{i+(d-1)\tau}\}, \tag{3}$$

where d is the embedding dimension and τ is the delay. There are standard methods devised to obtain reliable estimates from both d and τ [38]. For example, a good value of the delay is provided by the first zero of the auto-correlation function of the time series. The embedding dimension, on the other hand, can be estimated from the method of false neighbors.

It is convenient to regard the vectors $\mathbf{x}_i$ as belonging to a d-dimensional reconstructed phase space. Embedding theorems warrant that this reconstructed space reflects qualitative dynamical properties of the actual phase space of the system, provided d is large enough. However, even when d is a small number, we may retain essential and valuable information about the system's dynamics. The time evolution of the vector $\mathbf{x}_i$ can thus be represented by a trajectory in this reconstructed phase space.

We define a recurrence as the event where a trajectory visits roughly the same d-dimensional volume in the reconstructed phase space. A recurrence plot (RP) depicts, at a given instant, the times at which $\mathbf{x}_i \approx \mathbf{x}_j$, where $i = 1, 2, \cdots N$ (N is the total number of points) is represented in the horizontal axis, and j, with the same range, in the vertical axis. More formally, we construct a recurrence matrix by comparing embedding vectors with each others at different times, drawing pixels whenever the distance between vectors is within some threshold ϵ [27]

$$\mathbf{R}_{i,j} = \Theta(\epsilon - ||\mathbf{x}_i - \mathbf{x}_j||), \qquad i, j = 1, 2, \cdots N, \tag{4}$$

where $\Theta(.)$ is the Heaviside unit step function, and $||\cdots||$ stands for some norm, e.g. the Euclidean norm. The RP is thus obtained by assigning a black (white) dot to the points for which $\mathbf{R}_{i,j} = 1$ (0). By construction, the recurrence matrix is symmetric ($\mathbf{R}_{i,j} = \mathbf{R}_{j,i}$), and a point is always recurrent to itself, i.e. $\mathbf{R}_{i,i} = 1$, forming the main diagonal line. Diagonal lines, in general, are noteworthy features of RP, for they are consequences of the deterministic character of the dynamics generating the time series being investigated.

The higher the threshold ϵ, the more points are recurrent to other ones and the density of pixels increases. Hence, in order to warrant clearly distinguishable pixels in a RP, the threshold is usually chosen as a fraction, say 10%, of the time series variance. Moreover, other norms can be used (the maximum norm, for example) with minor modifications. Non-thresholded RPs can also be drawn, for which the step function in (4) is replaced by some smooth function with a color scale. We shall be concerned here, however, only to thresholded RPs.

Recurrences provide a systematic way to analyze the dynamical behavior of systems, even when the equations which govern their behavior are not known in advance. This applies well, for example, to situations involving plasma turbulence due to the extremely large dimensionality of the phase space. Moreover, as a complex system, the tokamak plasma has features of both

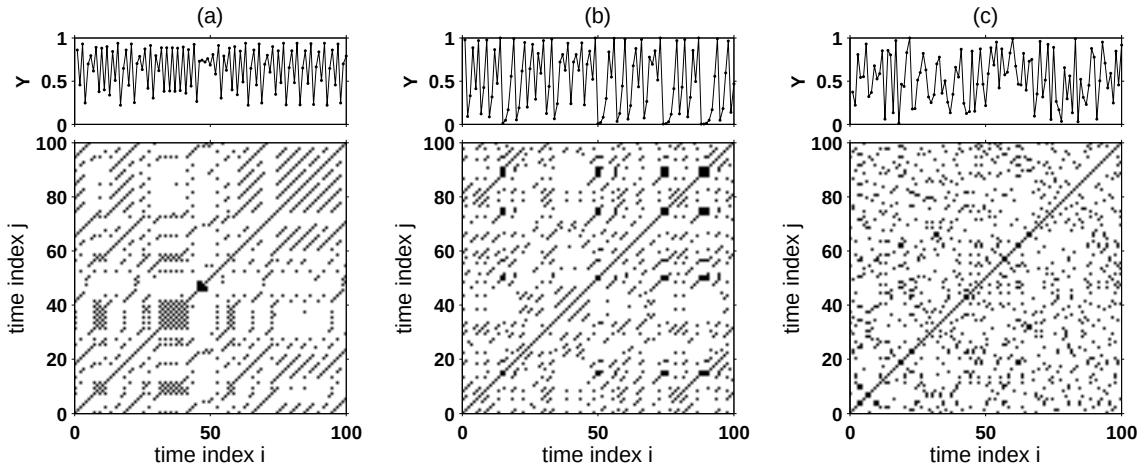

Figure 4. Time series (top) and corresponding recurrence plots (bottom) obtained from the logistic map $x \mapsto ax(1-x)$ with: (a) $a = 3.75$; (b) $a = 4.0$. In (c) we plot white noise obtained from a uniform distribution of random numbers in the interval $[0, 1]$.

deterministic and stochastic behavior, the dynamics alternating among various periodic, quasi-periodic, and chaotic states, with a pervading noise level of variable strength.

As a representative example of the usefulness of RPs for identifying dynamical regimes let us consider the logistic map $x_{n+1} = ax_n(1 - x_n)$, where $x \in [0, 1]$ and $a \in (0, 4]$, which is a well-known prototype of a low-dimensional dynamical system known to exhibit a wealth of dynamical phenomena, like periodic orbits, bifurcations, chaos, and crisis. When $a = 3.75$, for example, the time series for x_n displays an irregular (actually chaotic) dynamics [Fig. 4(a), top]. Its RP reflects the deterministic nature of this evolution, presenting many diagonal lines as well as isolated points which remind us of the irregularity of the time evolution [Fig. 4(a), bottom].

If a is raised to 4.0 in the logistic map, we know in advance that the time evolution is strongly chaotic (with Lyapunov exponent $\ln 2$, indeed), and the relative number of diagonal lines decreases in comparison with the previous case [Fig. 4(b)]. It is completely different, though, from white noise [Fig. 4(c)], which comes from a stochastic (non-deterministic) process (in this case, we considered pseudo-random numbers generated with a uniform probability distribution in the unit interval). In this case, diagonal lines are practically absent and chiefly isolated points are found (any recurrent point here would appear by chance). Hence RPs suggest a criterion for distinguishing chaos from noise in low-dimensional dynamical systems.

Dynamical regimes can be identified in RPs thanks to the existence of characteristic patterns, or structures, made of certain distributions of pixels. There are both large and small scale structures, which form a typology of dynamical behavior. Homogeneous RPs are typical of stationary series, for which the relaxation times are shorter than the series duration, as in a random time series, which is composed of scattered points uniformly distributed over the RP [Fig. 4(c)]. Periodic behavior is characterized by regularly distributed patterns in a checkerboard and diagonally oriented way. Abrupt changes or rare events manifest themselves as white bands, whereas drifted patterns are a fingerprint of non-stationary regimes, where system parameters may have suffered variations along the time series. Chaotic behavior has both structures and isolated points in variable proportions [Figs. 4(a) and (b)].

These features make RPs a useful tool for data analysis even when the time series is short, noisy, and non-stationary, which are commonly observed situations in fusion plasma experiments, specially turbulence data. The usefulness of RPs is further justified if we reckon that most of

dynamical diagnostics, like Lyapunov exponents, correlation dimensions, entropies, etc. require that data be long enough, stationary and corrupted with moderately weak noise. Recurrence plots are among the few dynamical diagnostics suitable for plasma turbulent fluctuations.

3.2. Recurrence quantification analysis

Recurrence quantification analysis (RQA) is a set of quantitative procedures to identify and characterize dynamical behavior using RPs, based in three basic kinds of structures: (i) isolated points; (ii) diagonal lines; (iii) horizontal and vertical lines. The first kind are single, or isolated points, which occur if the dynamical states are rare, do not persist for any time, or fluctuate heavily. Diagonal lines are sets of pixels parallel to the main diagonal line of the RP. They happen when finite segments of a trajectory run close to other segments for later times, which is a hallmark of recurrent behavior. Hence it is not surprising that the more diagonal lines are present, the more predictable is the system. The predictability of the further states given the actual state suggests a strong link with the presence of deterministic rules generating the time series. It is important to note that it is possible to generate predictable time series even using stochastic rules, then the link between the diagonal lines in the RPs and determinism is not unique. Finally, horizontal lines (or vertical lines which, due to the symmetry of RP, amounts to the same) occur when a system state does not change or change at a very slow pace, as in laminar states of intermittent behavior.

In order to quantify such structures, RQA provides a variety of numerical diagnostics. Two of the most important ones, namely the *determinism* and the *laminarity*, are described in the following, chiefly because they are used in this work. Several other measures can be found in the literature, and many of them are available in software packages [23].

The density of black recurrence points is a RP (for which $\mathbf{R}_{i,j} = 1$) is the *recurrence rate* (RR), or

$$RR = \frac{1}{N(N-1)} \sum_{i,j=1;i\neq j}^{N} \mathbf{R}_{i,j}, \tag{5}$$

where N^2 is the total number of pixels (black or white) in a RP, for a chosen data length. We remark that the main diagonal points are excluded from the double sum, since each point is recurrent with itself.

Diagonal lines of length ℓ can be formally defined as

$$\mathbf{R}_{i+k,j+k} = 1, \quad (k = 1, 2, \cdots, \ell), \quad \mathbf{R}_{i,j} = \mathbf{R}_{i+\ell+1,j+\ell+1} = 0, \tag{6}$$

and are parallel to the main diagonal line $R_{i,i} = 1$, $i = 1, 2, \cdots, N$. In a RP diagonal lines appear with various lengths, such that we compute $P(\ell) = \{\ell_i; i = 1, 2, \cdots N_\ell\}$, which is the frequency distribution of the lengths ℓ_i of diagonal lines, and N_ℓ is the absolute number of diagonal lines, with the exception of the main diagonal line which always exist by construction.

Since the presence of diagonal lines is usually linked with deterministic behavior, the percentage of points in a RP belonging to diagonal lines are called *determinism*. Accordingly we define the *determinism* (DET) as

$$DET = \frac{\sum_{\ell=\ell_{min}}^{\ell_{max}} \ell P(\ell)}{\sum_{\ell=1}^{\ell_{max}} \ell P(\ell)}, \tag{7}$$

where ℓ_{min} is the minimum length allowed for a diagonal line, whereas the *maximum diagonal length* is $\ell_{max} = max(\{\ell_i, i = 1, 2, \cdots N_\ell\})$.

Since the lengths of the diagonal lines measure locally the time it takes for two recurrent trajectories to depart from each other more than a given threshold ϵ, the diagonal line lengths

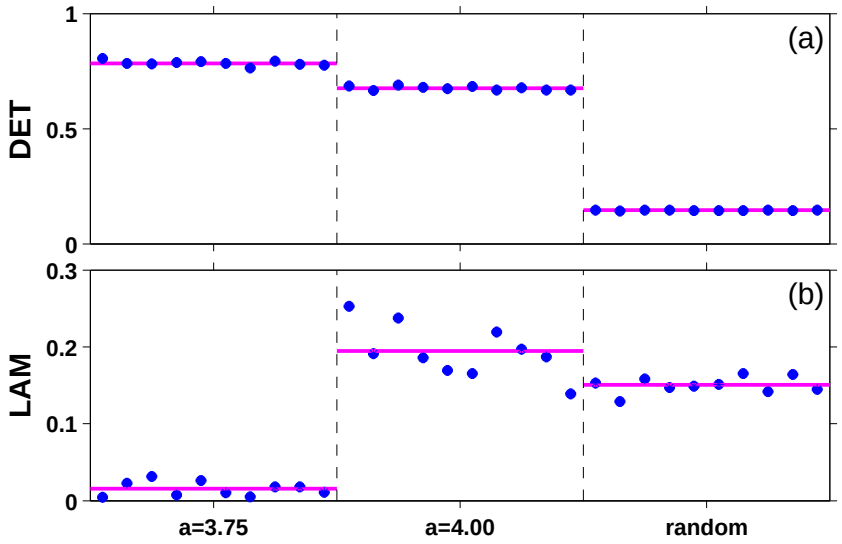

Figure 5. Determinism (a) and laminarity (b) of the time series shown in Figure 4. There were considered ten consecutive and non-overlapping windows of $1,000$ points each.

are related to the Lyapunov time, or the inverse of the largest positive Lyapunov exponent of the system. Hence periodic behavior, which has a large degree of predictability, is characterized by long diagonal lines. By way of contrast, a white noise, which has no predictability at all, would exhibit no more diagonal lines than those expected by pure chance. Chaotic systems, having both short and long diagonal lines as well as scattered isolated points, represent an intermediate kind of behavior, as is well-known in nonlinear dynamics.

Vertical lines of length v are defined by:

$$\mathbf{R}_{i,j+k} = 1, \quad (k = 1, 2, \cdots, v), \quad \mathbf{R}_{i,j} = \mathbf{R}_{i,j+v+1} = 0, \tag{8}$$

whose probability distribution function is denoted $P(v) = \{v_i; i = 1, 2, \cdots N_v\}$, where N_v is the absolute number of vertical lines. The *laminarity* (LAM) is the percentage of RP points forming vertical lines

$$LAM = \frac{\sum_{v=v_{min}}^{v_{max}} vP(v)}{\sum_{v=1}^{N_v} vP(v)}, \tag{9}$$

where v_{min} is the minimum lengths of a vertical line, whereas the maximum vertical length is $v_{max} = max(\{v_i, i = 1, 2, \cdots N_v\})$. Despite the vertical lines being related with laminar states of the system, the *laminarity* also can be used to characterize intermittency, since intermittent series are formed by a sequence of laminar states interspersed with bursts of irregular activity.

As an illustration of some of these quantifiers we plot in Figure 5 the values of DET and LAM corresponding to the time series depicted in Figure 4. We computed these quantifiers for ten consecutive and non-overlapping windows with $1,000$ points each. The absence of large fluctuations of DET and LAM along the time series is a compelling evidence for the stationarity. Indeed, these series are supposed to be stationary. In the first two cases the series come from a dynamical system (logistic map) with constant parameters, whereas in the third case the white noise has a time-independent mean and variance, which is a symptom of stationarity in stochastic data.

Moreover, the values of DET decrease as the time series goes from weakly chaotic (logistic map with $a = 3.75$) to completely random (white noise) [Fig. 5(a)], confirming that DET

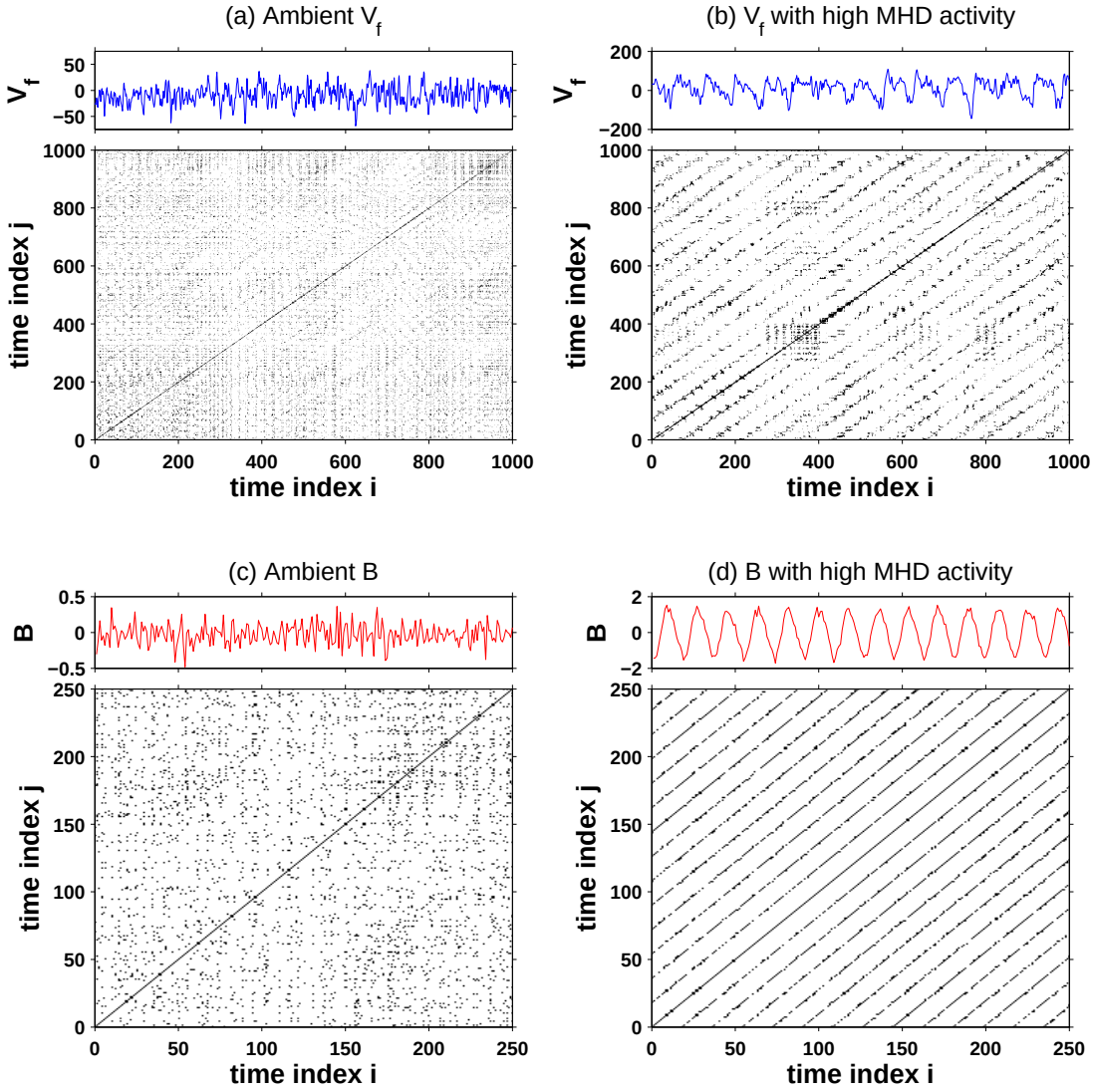

Figure 6. (color online) Recurrence Plots and correspondent time series of floating potential signals measured at $r/a = 0.94$ (for the same discharge showed in Fig. 1) during ambient (a) and high MHD activity (b) time intervals. The correspondents RPs for Mirnov oscillations are displaced in pictures (c) and (d).

measures our ability to detect the underlying determinism of the system generating the time series. A less evident measure is the laminarity LAM, as it does not display the same clearcut dependence on the deterministic character of the system from which the time series stems [Fig. 5(b)]. However, LAM can be useful if we are interested in the laminar behavior of a time series, as in the case when intermittent alternation exist between two states. In this work we mainly focus on DET.

3.3. Recurrence analysis of turbulence data

As we have seen, if the RP shows a cloud of points with a homogeneous yet irregular distribution, then the time series has a pronounced stochastic nature. On the other hand, the formation of

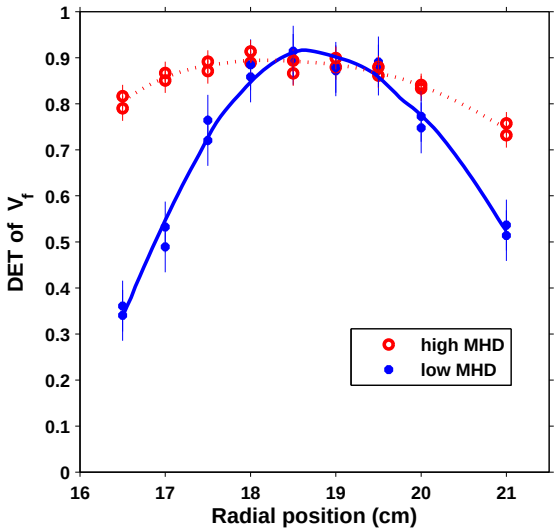

Figure 7. (color online) Radial profile of determinism of floating potential signals during high MHD activity (open red points). The blue points indicates the corresponding values during ambient MHD activity.

patterns in RPs may indicate stationary chaotic behavior. One example of changes in RPs can be seen in Fig. 6 for floating potential and magnetic signals measured at $r/a = 0.94$ (for the same discharge showed in Fig. 1) during ambient [Fig. 6(a),(c)] and high MHD activity [Fig. 6(b),(d)] time intervals. To compute these RPs, we choose the embedding dimension $m = 4$, and the time delay $\tau = 10$ μ s. We also choose the threshold ϵ for each RP to guarantee a fixed global density of black (recurrence) points. Is important to notice that the qualitative description does not depend much on these chosen parameters [24]. The deterministic content increases when we pass from $m = 1$ to 4, but saturates afterwards (see, by example, Figure 5 in [24]. We concluded that $m = 4$ is enough for our purposes. This does not imply that $m = 4$ is an optimal embedding dimension, in the sense we require, for example, for obtaining the correlation dimension through standard procedures [39], but recurrence plots with $m = 4$ already furnish results as good as with other higher-dimension (and time-consuming) embeddings.

While during the ambient MHD activity the RP is dominated by isolated points, during the high MHD activity structures can be observed aligned along the main diagonal in the RP. The structures present in the recurrence plots can be used to characterize the dynamical properties of the underlying time series [23]. One quantitative diagnostic of these structures is the determinism (DET), i.e., the fraction of recurrence points belonging to diagonal lines, which are structures parallel to the main diagonal line. Along a diagonal line, two pieces of a trajectory undergo for a certain time (the length of the diagonal) a similar evolution and visit the same region of phase space at different times. Hence the existence of many diagonal lines is a signature of determinism. The quantity DET is related with the predictability of the dynamical system, because a random process would have a recurrence plot with almost only single dots and very few diagonal lines, whereas a deterministic process has a recurrence plot with very few single dots but many long diagonal lines.

Thus, we perform this analysis and use the DET to estimate the change in the radial profile of the floating potential determinism. Figure 7 shows the DET radial profile for time intervals with ambient and high MHD activity. The obtained profile for ambient MHD activity has a maximum

near the plasma radius ($r/a \sim 1.05$) indicating a large deterministic turbulence component in this region. The effect of high MHD activity on the determinism of floating potential fluctuations is to uniformize the DET (in high values) for all analyzed region. In TCABR the scrape-off layer is large, presenting a high density gradient and indications of large scale structures [10, 18]. The increase of the determinism in this region is in favor of deterministic descriptions of plasma edge turbulence based on non-linear coupling of drift-waves, for which density gradients turn out to be an important source of energy. Moreover, the long scale structures are also indicated by the persistence of these signals, characterized by their Hurst exponent, that present a radial profile similar to the radial profile of determinism as shown in Fig. 7 of Reference [40].

4. Bicoherence analysis of turbulence data

The results presented in the previous section suggest the presence of nonlinear effects, as fluctuation couplings, in the analyzed fluctuations associated to high MHD activity. The standard procedure in time series analysis to detect and quantify the amount of mode coupling in a given turbulent signal is the bispectral analysis. Mode coupling results from nonlinear interactions which may be thought of as quadratic, in a first approximation. Thus, two modes with frequencies f_1 and f_2 can interact to generate a third mode with frequency f_3, which is phase-coupled to the other two modes. In this quadratic three-mode nonlinear process the mode frequencies must obey the resonance condition $f_1 + f_2 = f_3$. However, for regular oscillations, the phase differences between three modes can remain constant giving a high bicoherence value without any nonlinear coupling if their frequencies obey the resonant condition.

Let $\phi(f)$ be the Fourier transform of the time signal at the mode frequency f. The bispectrum is defined as [41, 42]

$$\mathcal{B}(f_1, f_2) = \langle \phi(f_1)\phi(f_2)\phi^*(f_3) \rangle \,, \tag{10}$$

which can be further normalized by introducing the associated bicoherence

$$b^2(f_1, f_2) = \frac{|\mathcal{B}(f_1, f_2)|^2}{\left\langle |\phi(f_1)\phi(f_2)|^2 \right\rangle \left\langle |\phi(f_3)|^2 \right\rangle}, \tag{11}$$

such that $0 \leq b^2 \leq 1$ and, accordingly, can be used as a measure of the amount of bicoherence between the modes in the triplet with frequencies f_1, f_2, and f_3. If the three modes are phase-coupled, there follows that b^2 is near the unity; whereas it is near zero if the modes are barely or no coupled at all.

Since we are quantifying the intensity of mode coupling in both electrostatic and magnetic time series, we shall distinguish them by using the following notations for the bicoherence: $b^2_{\varphi\varphi\varphi}$ and b^2_{BBB}, respectively. We present the bicoherence spectrum (in a grayscale for which darker shades of gray indicate larger values of b^2) as a function of the two frequencies f_1 and f_2 for magnetic and electrostatic signals in Figs. 8(a) and (b), respectively. We have chosen the time window (between 45 and 60 ms) corresponding to the occurrence of the major burst of spontaneous MHD activity [cf. Fig. 1(c)] in order to evidence the coupling between magnetic and electrostatic modes. The most pronounced peak of bicoherence in magnetic oscillations is centered at $f_1 = f_2 \approx 13$ kHz, indicating a strong coupling between these frequencies and a third mode with $f_3 \approx 26$ kHz. Other coupling can be detected in this way along a rough line of $f_2 \approx 13$ kHz. The second peak, centered at $f_1 \approx 26$ kHz, resonates with a third mode $f_3 \approx 39$ kHz and so on.

A similar picture is displayed in the bicoherence spectrum of electrostatic oscillations [Fig. 8(b)]. There is a line of high bicoherence along $f_1 \approx 13$ kHz, with peaks roughly at the same values as in the magnetic bicoherence. These bispectral similarities indicate a coupling between the electrostatic and magnetic fluctuations. The mentioned similarities are related

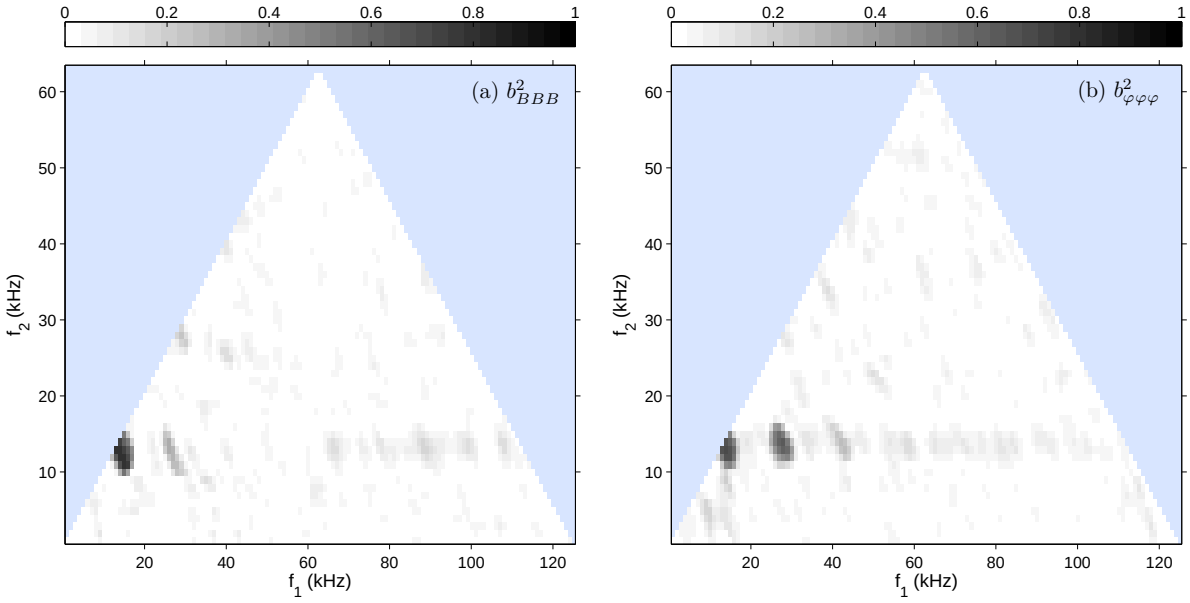

Figure 8. (color online) Bicoherence spectrum of (a) magnetic (b^2_{BBB}) and (b) electrostatic ($b^2_{\varphi\varphi\varphi}$) oscillations during high MHD activity (between 45 and 60 ms).

to prominent peaks in $f_1 = f_2 = 13$ kHz and their harmonics that appear in both magnetic and floating potential bicoherence spectra. A less intense but significative level of bicoherence between ambient turbulence and driven frequency (13 kHz) is seen in the coupling involving the continuous part of bicoherence spectrum with frequencies above the peaks region. In order to investigate the radial dependence of the coupling between electrostatic and magnetic fluctuations we plot in Fig. 9 the radial profile of the maximum values of the bicoherence for floating potential (points) during the high magnetic activity.

According to Fig. 9 the strength of bicoherence for electrostatic potential fluctuation increases as we approach a maximum radius of 17 cm, one centimeter before the plasma column radius, and decreases afterwards to a minimum value at the scrape off layer. The behavior is essentially the same for the ion saturation current measurements [19]. It is remarkable that this radial dependence only occurs during the strong MHD activity, since the corresponding values of the maximum bicoherence without magnetic activity are very low [indicated by a dashed line in Fig. 9]. This may be regarded as a consequence of coupling of electrostatic and magnetostatic oscillations. The radial position of this maximum agrees with the position with the higher value of the synchronization intensity, and is similar to the 3/1 resonant magnetic surface position. However, the radial position of the bicoherence maximum does not coincide with the position of the maximum determinism during high MHD activity (at $r \approx 18$ cm). This difference suggests that the observed recurrence structures are not determined by the mode coupling only.

The foregoing data analysis could be well simulated by a chaotic dynamical system based on three coherent coupled modes with an incoherent noise and a nonlinear periodic driven, which plays the role of a source on the MHD frequency [19]. A better physical interpretation of this forcing would require solving basic equations describing coupled magnetic and electrostatic oscillations under the conditions of the analyzed experiments [43].

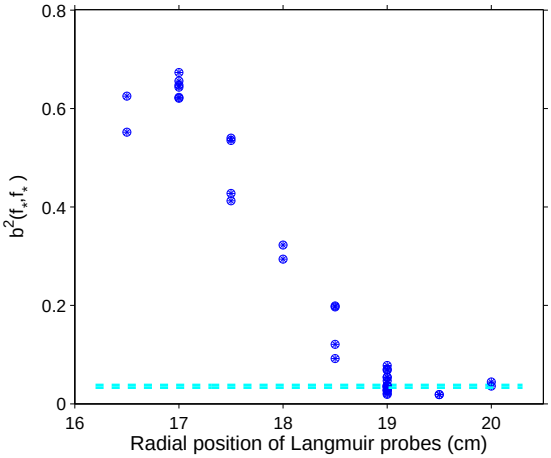

Figure 9. (color online) Radial profile of the maximum bicoherence spectra of floating potential signals (points). The dashed line indicate the corresponding values for periods of ambient MHD activity (reproduced from Fig. 4(b) of Ref. [19]).

5. Conclusions

Previous works have shown that, during TCABR tokamak discharges with high MHD activity, the electrostatic plasma edge turbulence and the turbulence driven particle transport are strongly influenced by the MHD activity at its dominant frequency [10, 16, 17]. This high magnetic activity can be obtained in two different regimes of TCABR discharges. In one regime, the enhancement of MHD activity was observed only after the activation of a biasing electrode while, in the other regime, this enhancement occurs spontaneously [17]. In this article, we considered the second TCABR regime, and reported dynamical characteristics of electrostatic plasma edge turbulence that are clearly changed by the MHD activity enhancement. Namely, in these discharges, (i) high MHD activity and the electrostatic turbulence synchronize at the MHD frequency, (ii) the recurrence structures change broadening the radial profile of plasma with high determinism, and (iii) the bicoherence involving the dominant MHD frequency increases inside plasma nearest to edge.

The recurrence quantification analysis shows that the changes in the recurrence structures can be observed in whole plasma edge region, clearly indicating that these structures are determined by the high MHD activity. On the other hand, by applying the bicoherence analysis to the TCABR Langmuir probe and Mirnov coil data, we identified similar bicoherence spectra with noticeable high values related to the MHD frequency. For the electrostatic turbulence it was possible to obtain the radial profile of the coupling strength, with a local maximum near the estimated 3/1 resonant magnetic flux surface radial position.

In comparing the results of analyses reported in this article we claim that, while the recurrence quantification analysis shows the alterations on the recurrence structures of turbulence, the bicoherence evidences the nonlinear coupling in both magnetic and turbulence fluctuations during high MHD activity. Furthermore, RQA indicates that the structure alterations occur throughout the whole edge region, thus requiring a model to describe the onset and propagation of perturbing structures that consider both the plasma edge and the scrape-off layer regions. The bicoherence alterations, for other hand, are radially localized and gives us indication about the position of the coupling between the magnetic and turbulent fluctuations.

The amplitude dependent synchronization on specific frequencies considered in this article is

commonly observed in other experimental nonlinear dynamical systems, as in chaotic electronic circuits perturbed by AC tensions [44, 36, 45]. Recently this kind of synchronization has also been observed in some plasma discharges in linear devices perturbed by time-periodic electric potentials [46, 47, 48]. Thus, the above mentioned observations in TCABR can be interpreted as an indication of an onset of nonlinear coupling between the magnetic and the electric fluctuations during periods of high MHD activity.

We conjecture that a nonlinear coupling modifies the turbulence until it assumes the observed similarities. Thus, we may be observing the turbulence final state and not the turbulence transition driven by high MHD activity. Other interpretations could also be considered to explain the observed spectrum and bispectrum similarities. For instance, an interaction between a saturated nonlinear tearing mode and the turbulence, that modifies the equilibrium so as to include large magnetic islands [3, 49]. Another possibility would be to associate the onset of high MHD activity during some TCABR discharges to the generation of electromagnetic non-normal modes in drift-wave-zonal flow turbulence, as predicted in [50, 51].

Acknowledgements

This work was made possible with partial financial help from FAPESP, CNPq, CAPES, FINEP/CNEN (Brazilian Fusion Network), Fundação Araucária (Paraná), Université de Provence and PACA (Provence Alpes Côte d'Azur) Region. Z.O.G.-F. is recipient of a bourse d'accueil de la Ville de Marseille. The authors acknowledge useful discussions with J. Kurths.

References

[1] Horton W 1999 *Rev. Mod. Phys.* **71** 735
[2] Hidalgo C *et al* 2005 *Nucl. Fusion* **45** S266
[3] Pedrosa M A *et al* 2007 *Plasma Phys. Control. Fusion* **49** B303
[4] Conway G D 2008 *Plasma Phys. Control. Fusion* **50** 124026
[5] Finken K H, Evans T E, Reiter D, Spatschek K H and Suttrop W 2008 *Nucl. Fusion* **48** 024001
[6] Tokar M Z, Evans T E, Singh R and Unterberg B 2008 *Phys. Plasmas* **15** 072515
[7] Schaffer M J, Menard J E, Aldan M P, Bialek J M, Evans T E and Moyer R A 2008 *Nucl. Fusion* **48** 024004
[8] Schmitz O *et al* 2008 *Nucl. Fusion* **48** 024009
[9] Lin H 1991 *Turbulence and transport studies in the edge plasma of the TEXT tokamak* Ph.D. Thesis, Report FRCR/401, University of Texas, Fusion Rechearch Center, Austin, TX, USA
[10] Heller M V A P, Castro R M, Brasílio Z A, Caldas I L and Silva R P 1995 *Nucl. Fusion* **35** 59
[11] Devynck P *et al* 2005 *Plasma Phys. Control. Fusion* **47** 269
[12] Heller M V A P, Caldas I L, Ferreira A A, Saettone E A O and Vannucci A 2007 *J. Plas. Phys.* **73** 295
[13] Heller M V A P, Caldas I L, Ferreira A A, Saettone E A O, Vannucci A, Nascimento I C and Severo J H F 2005 *Czech. J. Phys.* **55** 1572
[14] Sharapov S E *et al* 2008 *Europhysics Conference Abstracts* (35th EPS Conference on Plasma Physics, Hersonissos) eds P Lalousis and S Moustaizis (European Physical Society) vol 32D pp P-4.071
[15] Perez J C, Horton W, Bengtson R D and Carter T 2006 *Phys. Plasmas* **13** 055701
[16] Nascimento I C *et al* 2005 *Nucl. Fusion* **45** 796
[17] Nascimento I C *et al* 2007 *Nucl. Fusion* **47** 1570
[18] Guimarães-Filho Z O, Caldas I L, Viana R L, Heller M V A P, Nascimento I C, Kuznetsov Y K and Bengtson R D 2008 *Phys. Plasmas* **15** 062501
[19] Lima G Z S, Guimarães-Filho Z O, Batista A M, Caldas I L, Lopes S R, Viana R L, Nascimento I C and Kuznetsov Y K 2009 *Phys. Plasmas* **19** 042508
[20] Yan L W *et al* 2005 *Nucl. Fusion* **47** 1673
[21] Nagashima Y *et al* 2005 *Phys. Rev. Lett.* **95** 095002
[22] Pedrosa M A *et al* 2008 *Phys. Rev. Lett.* **100** 215003
[23] Marwan N, Romano M C, Thiel M and Kurths J 2007 *Phys Rep.* **438** 237
[24] Guimarães-Filho Z O, Caldas I L, Viana R L, Kurths J, Nascimento I C and Kuznetsov Y K 2008 *Phys. Lett.* A **372** 1088
[25] Guimarães-Filho Z O, Caldas I L, Viana R L, Nascimento I C, Kuznetsov Y K and Kurths J 2010 *Phys. Plasmas* **17** 012303

[26] Zivkovic T and Rypdal K 2008 *Phys. Rev.* E **77** 037401
[27] Eckmann J P, Kamphorst S O and Ruelle D 1987 *Europhys. Letters* **4** 963
[28] Casdagli M 1997 *Physica* D **108** 12
[29] Webber C L and Zbilut J P 1994 *J. Appl. Physiol.* **76** 965
[30] Marwan N, Trauth M H, Vuille M and Kurths J 2003 *Climate Dynamics* **21** 317
[31] Holyst J A , Zebrowska M and Urbanowicz K 2001 *Eur. J. Phys.* B **20** 531
[32] Kurths J, Schwarz U, Sonett C P and Parlitz U 1994 *Nonlinear Processes in Geophysics* **1** 71
[33] Marwan N, Wessel N, Meyerfeldt U, Schirdewan A and Kurths J 2002 *Phys. Rev.* E **66** 026702
[34] March T K, Chapman S C and Dendy R O 2005 *Physica* D **200** 171
[35] Pinto S E S and Viana R L 2000 *Phys. Rev.* E **61** 5154
[36] Baptista M S, Pereira T, Sartorelli J C, Caldas I L and Kurths J 2005 *Physica* D **212** 216
[37] Takens F 1980, in *Dynamical Systems and Turbulence* eds D A Rand and L S Young, Springer Lecture Notes in Mathematics, vol 898 (New York: Springer)
[38] Kantz H and Schreiber T 1997 *Nonlinear Time Series Analysis* (Cambridge: Cambridge University Press)
[39] Grassberger P and Procaccia I 1983 *Physica* D **9** 189
[40] Rodrigues Neto C, Guimares-Filho Z O, Caldas I L, Nascimento I C and Kuznetsov Y K 2008 *Phys. Plasmas* **15** 082311
[41] Ritz C P *et al* 1988 *Rev. Sci. Instrum.* **59** 1739
[42] Milligen B P, Sánchez E, Estrada T, Hidalgo C , Brañas B, Carreras B and García L 1995 *Phys. Plasmas* **2** 3017
[43] Beyer P, Garbet X and Ghendrih P 1998 *Phys. Plasmas* **5** 4271
[44] Baptista M S, Silva T P, Sartorelli J C and Caldas I L 2003 *Phys. Rev.* E **67** 056212
[45] Baptista M S, Garcia S P , Dana S K and Kurths J 2008 *Eur. Phys. J.* **165** 119
[46] Ticos C M, Rosa Jr E, Pardo W B , Walkenstein J A, Monti M 2000 *Phys. Rev. Lett.* **85** 2929
[47] Davis M S, Nutter N G , Rosa Jr E 2007 *Int. J. Bifurcat. Chaos* **17** 3513
[48] Schröder C, Klinger T, Block D, Piel A , Bonhomme G , Naulin V 2001 *Phys. Rev. Lett.* **86** 5711
[49] Militello F, Waelbroeck F L, Fitzpatrick R and Horton W 2008 *Phys. Plasmas* **15** 050701
[50] Camargo S J, Tippett M and Caldas I L 1998 *Phys. Rev.* E **58** 3693
[51] Horton W, Correa C, Chagelishvili G D, Avsarkisov V S, Lominadze J G, Perez J C, Kim K H and Carter T A 2009 *Phys. Plasmas* **16** 092102